Theoretical and Synthetic Studies on Dihaptoacyl and β-Agostic Acyl Complexes of Molybdenum

Gregori Ujaque, Feliu Maseras, and Agustí Lledós*

Departament de Química, Universitat Autònoma de Barcelona, 08193 Bellaterra, Barcelona, Spain

Leopoldo Contreras, Antonio Pizzano, Dieter Rodewald, Luis Sánchez,* and Ernesto Carmona*

Instituto de Investigaciones Químicas-Departamento de Química Inorgánica, CSIC-Universidad de Sevilla, 41092 Sevilla, Spain

Angeles Monge and Caridad Ruiz

Instituto de Ciencia de Materiales de Madrid, CSIC, Cantoblanco, E-28049 Madrid, Spain

Received August 26, 1998

Molybdenum acyl complexes of formula $Mo(C(O)CH_2SiMe_2R)(S_2CX)(CO)(PMe_3)_2$ (R = Me, Ph; X = NMe_2 (**2-Me**, **2-Ph**), N-*i*-Pr_2 (**3-Me**), NC_4H_4 (**4-Me**), O-*i*-Pr (**5-Me**, **5-Ph**), O-*t*-Bu (**6-Me**)) containing several S-donor ligands have been prepared and characterized. Compounds **2-Me** and **2-Ph** exist in solution as equilibrium mixtures of the agostic and the dihaptoacyl species and crystallize, respectively, as the isomeric mixture (**2-Me**) and as the agostic compound (**2-Ph**). Complexes **3**−**6** show dihapto coordination both in solution and in the solid state. Confirmation of the agostic coordination of the Mo-acyl moiety has been provided by an X-ray diffraction study of $Mo(\overline{C(O)CH_2}SiMe_3)(S_2CNMe_2)CO(PMe_3)_2$ and by ab initio calculations performed with the representative model species $Mo(C(O)CH_2R)(S_2CNH_2)(CO)(PH_3)_2$ (R = H (**8**), SiH_3 (**9**)), which show good agreement with the structural data of the parent compounds. For **8** a value of 12.7 kcal mol^{-1} has been obtained for the agostic stabilization. Calculation of the energy profile for the CO deinsertion in **8** gives an energy barrier of 4.0 kcal mol^{-1} for the C_α-C_β breaking process, in good accordance with the available experimental data.

Introduction

The insertion of carbon monoxide into a metal-alkyl bond is a fundamental organometallic reaction.[1] The seemingly unrelated nonclassical $\overline{M\text{-}C\text{-}H}$ interaction, i.e., agostic interaction,[2] plays a key role in some important organometallic transformations (e.g. C−H activation[3] and olefin polymerization[4]) but also in the stabilization of unsaturated intermediates.[5] Some years ago, we reported the formation of the first agostic acyl complex of a transition metal, $Mo(\overline{C(O)CH_3})(S_2CNMe_2)$-$CO(PMe_3)_2$,[6a] and suggested that the severely distorted **Mo**−$\mathbf{C}_\alpha$−$\mathbf{C}_\beta$ angle it presented (structure **a**, Figure 1) could be considered as a model for the transition state, or intermediate of the CO insertion reaction into M−C bonds. This apparent connection between migratory CO

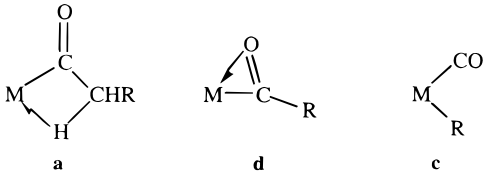

a d c

Figure 1.

(1) (a) Parshall, G. W.; Ittle, S. D. *Homogeneous Catalysis*, 2nd ed.; Wiley-Interscience: New York, 1992. (b) Collman, J. P.; Hegedus, L. S.; Norton, J. R.; Finke, R. G. *Principles and Applications of Organotransition Metal Chemistry*; University Science Books: Mill Valley, CA, 1987.

(2) (a) Brookhart, M.; Green, M. L. H. *J. Organomet. Chem.* **1983**, *250*, 395. (b) Brookhart, M.; Green, M. L. H.; Wong, L.-L. *Prog. Inorg. Chem.* **1988**, *36*, 1.

(3) (a) Gleiter, R.; Hyla-Kryspin, I.; Niu, S.; Erker, G. *Organometallics* **1993**, *12*, 3828. (b) Crabtree R. H. *Angew. Chem., Int. Ed. Engl.* **1993**, *32*, 789.

(4) (a) Grubbs, R. H.; Coates, G. W. *Acc. Chem. Res.* **1996**, *29*, 85. (b) Brintzinger, H. H.; Fischer, D. F.; Mülhaupt, R.; Rieger, B.; Waymouth, R. *Angew. Chem., Int. Ed. Engl.* **1995**, *34*, 1143. (c) Tanner, M. J.; Brookhart, M.; DeSimone, J. M. *J. Am. Chem. Soc.* **1997**, *119*, 7617. (d) Schmidt, G. F.; Brookhart, M. *J. Am. Chem. Soc.* **1985**, *107*, 1443. (e) Han, Y.; Deng, L.; Ziegler, L. *J. Am. Chem. Soc.* **1997**, *119*, 5939.

(5) (a) Jordan, R. F.; Bradley, P. K.; Baenzinger, N. C.; Lapointe, R. E. *J. Am. Chem. Soc.* **1990**, *112*, 1289. (b) Brookhart, M.; Lincoln, D. M.; Bennett, M. A.; Pelling, S. *J. Am. Chem. Soc.* **1990**, *112*, 2691. (c) Conroy-Lewis, F. M.; Mole, L.; Redhouse, A. D.; Litster, S. A.; Spencer, J. L. *J. Chem. Soc., Chem. Commun.* **1991**, 1601. (d) Cracknell, R. B.; Orpen, A. G.; Spencer, J. L. *J. Chem. Soc., Chem. Commun.* **1984**, 326. (e) Turner, H. W.; Schrock, R. R. *J. Am. Chem. Soc.* **1983**, *105*, 4942. (f) Feng, S. G.; White, P. S.; Templeton, J. L. *J. Am. Chem. Soc.* **1990**, *112*, 8192.

(6) (a) Carmona, E.; Sánchez, L.; Marín, J. M.; Poveda, M. L.; Atwood, J. L.; Priester, R. D.; Rogers, R. D. *J. Am. Chem. Soc.* **1984**, *106*, 3214. (b) Carmona, E.; Contreras, L.; Poveda, M. L.; Sánchez, L. *J. Am. Chem. Soc.* **1991**, *113*, 4322. (c) Contreras, L.; Monge, A.; Pizzano, A.; Ruiz, C.; Sánchez, L.; Carmona, E. *Organometallics* **1992**, *11*, 3971.

10.1021/om9807248 CCC: $18.00 © 1999 American Chemical Society
Publication on Web 07/20/1999

Scheme 1

$$\mathrm{Mo(\eta^2\text{-}C(O)CH_2SiMe_2R)Cl(CO)(PMe_3)_3} \xrightarrow[-MCl,\ -PMe_3]{M[S_2CX]} \mathrm{Mo(C(O)CH_2SiMe_2R)(S_2CX)(CO)(PMe_3)_2}$$

(R = Me, Ph)

X = NMe_2, **2**; N-*i*-Pr_2, **3**; NC_4H_4, **4**; O-*i*-Pr, **5**; O-*t*-Bu, **6**

insertion and agostic M−C−H interactions has been noted by others. Thus, time-resolved infrared and optical spectroscopy studies have considered agostic acyls as plausible alternatives to solvent stabilized- or dihaptoacyl intermediates,[7] whereas a recent theoretical investigation of the carbonylation of CH_4 by the model catalyst $RhCl(CO)(PH_3)_2$ has shown that the transition state for the migratory insertion step is stabilized by the formation of a β-agostic $RhC(O)CH_3$ bond.[8]

For reasons that remain unknown to us, the experimental observation of agostic acyls is still restricted to Mo complexes of composition $Mo(\overline{C(O)CH_3})(S_2CX)CO(PMe_3)_2$, prepared and characterized in our laboratories.[6] This series of complexes has been demonstrated to be particularly suitable for studying the preference for the agostic coordination (**a**) over the dihaptoacyl (**d**) or the alkyl-carbonyl formulations (**c**), since the relative stabilities of these isomeric structures appear to depend in solution upon the nature of the bidentate, monoanionic S_2CX ligand. For instance, compounds that incorporate bulky and strongly electron-releasing dialkyldithiocarbamate groups exist in solution as equilibrium mixtures between the **a** and **c** type compounds while the alkylxanthate derivatives show in addition the presence of the dihapto compound of type **d**. Contrarily, the analogous complex of the less-donating 1-pyrrolyl dithiocarbamate group exists in solution as the **d** isomer only.

With the aim of improving our knowledge on the factors that govern the adoption of structure **a** we present here an extension to our previous work with molybdenum acyls. The synthesis and characterization of silyl derivatives of composition $Mo(C(O)CH_2SiMe_2R)(S_2CX)CO(PMe_3)_2$ (R = Me, Ph; S_2CX = alkyl xanthate or dialkyldithiocarbamate) are described, as well as spectroscopic studies of their behavior in solution. Additional structural evidence for the agostic coordination is given by a new X-ray crystallographic study and valuable complementary information is provided by the results of a theoretical analysis of the metal-acyl interaction by ab initio methods.

Results and Discussion

Synthesis of the Acyls $Mo(C(O)CH_2SiMe_2R)(S_2CX)(CO)(PMe_3)_2$ (R = Me, Ph). X-ray Structure of the Agostic Complex $Mo(\overline{C(O)CH_2SiMe_3})(S_2CNMe_2)CO(PMe_3)_2$, 2a-Me. Reaction of the alkaline salts (Na^+ or K^+) of several dialkyldithiocarbamate and alkylxanthate ligands, in diethyl ether (Et_2O) or tetrahydrofuran (THF), with the chloro(acyl) complexes $Mo(\eta^2\text{-}C(O)CH_2SiMe_2R)Cl(CO)(PMe_3)_3$ (R = Me, **1-Me**; Ph, **1-Ph**) produces incorporation of the dithio acid ligand with concomitant release of the chloride and one of the groups PMe_3 and formation of the acyl derivatives **2**−**6** (Scheme 1). As shown in Scheme 1, the new acyls are designated by numbers from **2** to **6**, according to the nature of the dithio acid ligand. Since two different R groups have been employed, they are further denoted with the appropriate **Me** or **Ph** symbol. In some instances two isomeric possibilities may be observed, namely the dihaptoacyl structure of type **d** (see above) or the agostic formulation **a**, hence these letters will additionally be used when appropriate.

With the exception of compound **5-Ph**, obtained as an oily, albeit spectroscopically pure material, complexes **3**−**6** are isolated as orange-red crystalline solids of the dihapto isomer. In contrast, acyl **2-Me** crystallizes from its solutions in Et_2O-petroleum ether mixtures as a mixture of the agostic isomer **2a-Me** (yellow-orange) and the dihapto compound **2d-Me** (orange-red). Careful crystallization, or even manual separation of the crystalline mixture, allows the separation of the two isomers. The phenyl derivative **2-Ph** seems to crystallize exclusively as the agostic form, even though the dihapto complex predominates in solution (vide infra). They are all moderately stable to air in the solid state, but very sensitive in solution. In particular they demonstrate easy C−Si heterolysis[9] in the presence of adventitious water, to generate the compounds $Mo(C(O)CH_3)(S_2CX)CO(PMe_3)_2$, previously described by our group.[6]

The coordination mode of the acyl fragment in the above complexes can be readily identified from their IR spectra (Nujol mull). Thus derivatives **3d**−**6d** show two bands in the carbonyl region: a strong absorption in the interval 1800−1750 cm^{-1} due to ν(CO) of a terminal carbonyl ligand; and a medium intensity band in the 1490−1465 cm^{-1} range, characteristic of an acyl fragment coordinated in the dihapto fashion.[10] Contrary to the acyl fragment spectra, the agostic isomers **2a-Me** and **2a-Ph**, in which back-donation to the C═O fragment is absent, present the corresponding band as a fairly strong absorption at 1615 and 1598 cm^{-1} respectively.

Further insight into the agostic nature of the interaction between the acyl fragment and the metal center in these compounds has been gained from an X-ray study carried out with the **2a-Me** derivative. Suitable crystals of this compound have been obtained by careful crystallization of its solutions in Et_2O. Figure 2 shows an ORTEP diagram of its molecules, while Tables 1 and 2 display crystallographic data and some selected bond distances and angles, respectively. The geometry of **2a-Me** clearly resembles the molecular structure of other agostic acyls studied previously in our laboratory.[6] If the acyl group is considered to occupy a single coordina-

(7) (a) Boese, W. T.; Ford, P. C. *J. Am. Chem. Soc.* **1995**, *117*, 8381. (b) Boese, W. T.; Lee, B.; Ryba, D. W.; Belt, S. T.; Ford, P. C. *Organometallics* **1993**, *12*, 4739.

(8) (a) Margl, P.; Ziegler, T.; Blöchl *J. Am. Chem. Soc.* **1996**, *118*, 5412.

(9) For other C−Si heterolyses, see for example: (a) Carmona, E.; Contreras, L.; Gutiérrez-Puebla, E.; Monge, A.; Sánchez, L. J. *Organometallics* **1991**, *10*, 71. (b) Allen, S. R.; Green, M.; Orpen, A. G.; Williams, I. D. *J. Chem. Soc., Chem. Commun.* **1982**, 826.

(10) Although the value of ν(CO) cannot be taken as diagnostic of dihapto coordination, confident assignment can be made along a series of similar compounds: Durfee, L. D.; Rothwell, I. P. *Chem. Rev.* **1988**, *88*, 1059.

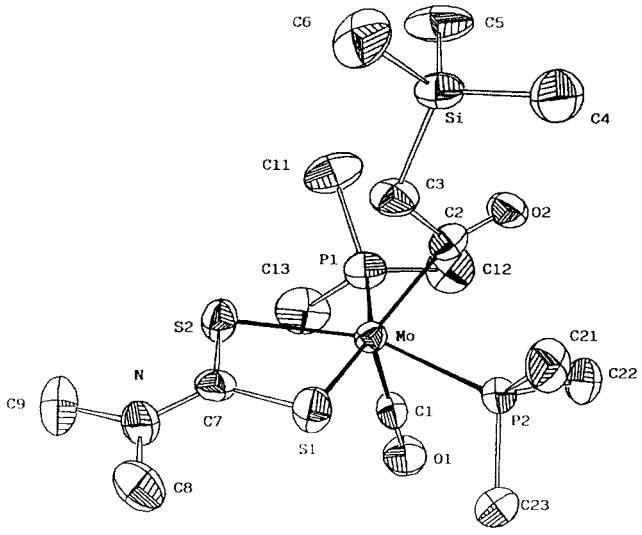

Figure 2. ORTEP diagram of $Mo(C(O)CH_2SiMe_3)(S_2CNMe_2)CO(PMe_3)_2$ (**2a-Me**).

Table 1. Crystal and Refinement Data for 2a-Me

formula	$MoS_2P_2SiO_2NC_{15}H_{35}$
M_r	511.5
cryst syst	orthorhombic
space group	$P2_12_12_1$
a, Å	9.338(4)
b, Å	12.480(3)
c, Å	21.103(9)
V, Å^3	2459(2)
Z	4
F(000)	1064
ρ(calcd), g cm^{-3}	1.38
temp, °C	22
μ, cm^{-1}	8.7
cryst dimens, mm	0.1 × 0.1 × 0.2
diffractometer	Enraf-Nonius CAD4
radiation	graphite-monochromated Mo Kα (λ = 0.710 69 Å)
scan technique	$\Omega/2\theta$
data collected	(−11, 0, 0) to (11, 15, 26)
no. of rflcns collcd	5418
no. of unique data	2748
no. of unique data, $(I) \geq 2\sigma(I)$	2290
R(int), %	4.1
no. of std rflcns	3
$R(F)$, %	3.7
R_w(F), %	5.5
average shift/error	0.08

tion site, the geometry of **2a-Me** can be regarded as derived from a distorted octahedron, with the chelating dithio acid ligand and the two trimethylphosphine fragments occupying the equatorial plane, and the carbonyl functionalities, i.e., the terminal carbonyl ligand and the agostic acyl moiety, positioned in the axial sites. The geometry of the coordinated acyl ligand deserves specific comment. The interaction between the metal and the terminal CH_2R group of the acyl ligand produces a severe distortion with respect to the geometry characteristic of the monohaptoacyl fragment, M−C(O)R, clearly denoted by the value of the angle Mo−C(2)−C(3) of 94.7(6)°. This is significantly shorter than the value of 120.9° observed in $CpMo(\eta^1\text{-}C(O)CH_3)(CO)_2PPh_3$.[11] Since the angle formed by the O(2), C(2), and C(3) atoms (117.2(9)°) remains close to the ideal value expected for an sp^2 hybridation at C(3), the approach of one of the β-C(3)−H bonds can be envisioned as a pivotating of the acyl ligand from the monohapto coordination, to bring the carbon atom C(3) closer to the Mo atom. This originates the agostic interaction (or agostic distortion, vide infra) characterized by Mo−C(3) and Mo−H(32) distances of 2.69(11) and 2.65(9) Å, respectively. These values lie well in the range observed for other agostic acyls and do not require further comment. Also very characteristic of the agostic acyl interaction are the values of the Mo−C(2)−O(2) and Mo−C(2)−C(3) angles (148.1(8) and 94.7(6)° respectively). They are in the intervals expected for this type of coordination but, as already discussed at length,[6] differ considerably from those corresponding to the η^1- and η^2-acyl structures. Finally, it should be noted that the formal substitution of a H atom of the $C(O)CH_3$ fragment by a $SiMe_3$ unit does not introduce any significant variation in the structural parameters of these complexes.

Table 2. Selected Bond Distances and Angles for 2a-Me

Mo−P1	2.432(3)	Si−C3	1.873(11)
Mo−P2	2.413(3)	Si−C4	1.859(15)
Mo−S1	2.526(3)	Si−C5	1.868(14)
Mo−S2	2.528(3)	Si−C6	1.845(15)
Mo−C1	1.864(11)	S1−C7	1.710(11)
Mo−C2	2.045(11)	S2−C7	1.710(11)
P1−C11	1.822(14)	O1−C1	1.218(14)
P1−C12	1.785(15)	O2−C2	1.214(13)
P1−C13	1.839(14)	N−C7	1.324(13)
P2−C21	1.831(13)	N−C8	1.466(19)
P2−C22	1.815(12)	N−C9	1.460(16)
P2−C23	1.822(13)	C2−C3	1.587(15)
C1−Mo−C2	120.1(4)	Mo−P2−C21	116.7(4)
S2−Mo−C2	121.3(3)	C22−P2−C23	102.3(6)
S2−Mo−C1	108.0(3)	C21−P2−C23	100.8(6)
S1−Mo−C2	118.2(3)	C21−P2−C22	102.3(6)
S1−Mo−C1	108.6(3)	C5−Si−C6	107.2(6)
S1−Mo−S2	70.0(1)	C4−Si−C6	110.5(6)
P2−Mo−C2	74.9(3)	C4−Si−C5	109.5(6)
P2−Mo−C1	76.0(3)	C3−Si−C6	105.5(6)
P2−Mo−S2	152.7(1)	C3−Si−C5	112.8(6)
P2−Mo−S1	83.0(1)	C3−Si−C4	111.1(6)
P1−Mo−C2	75.3(3)	Mo−S1−C7	86.6(4)
P1−Mo−C1	75.7(3)	Mo−S2−C7	86.5(4)
P1−Mo−S2	86.9(1)	C8−N−C9	116.0(9)
P1−Mo−S1	156.9(1)	C7−N−C9	121(1)
P1−Mo−P2	119.7(1)	C7−N−C8	122.0(9)
Mo−P1−C13	114.5(5)	Mo−C1−O1	179.2(9)
Mo−P1−C12	116.5(5)	Mo−C2−O2	148.1(8)
Mo−P1−C11	117.5(5)	O2−C2−C3	117.2(9)
C12−P1−C13	102.5(6)	Mo−C2−C3	94.7(6)
C11−P1−C13	100.8(6)	Si−C3−C2	114.3(7)
C11−P1−C12	102.7(7)	S2−C7−N	123.1(8)
Mo−P2−C23	114.0(4)	S1−C7−N	120.7(8)
Mo−P2−C22	118.2(5)	S1−C7−S2	116.0(6)

Structural and Electronic Features of $Mo(C(O)CH_2R)(S_2CX)(CO)(PMe_3)_2$ Agostic Complexes. Theoretical calculations were carried out on a number of model systems of experimentally reported acyl complexes. The modeling always consisted of the replacement by hydrogen atoms of substituents remote from the metal-acyl interaction. In this way, PMe_3 ligands were modeled as PH_3, and the $SiMe_3$ substituent as SiH_3. Calculations were carried out on the parent complex $Mo(C(O)CH_3)(S_2CNMe_2)CO(PMe_3)_2$ (**7**)[6a] and on the species reported here $Mo(C(O)CH_2SiMe_3)(S_2CNMe_2)$-

(11) Churchill, M. R.; Fennessey, J. P. *Inorg. Chem.* **1968**, *7*, 953.

Table 3. Relevant Structural Parameters (in Å and deg) of $Mo(COCH_2R)(S-S)(CO)(PR_3)_2$ Agostic Complexes[a]

	7[b] X-ray	**8** opt.	**2a-Me** X-ray	**9** opt.	**10**[c] X-ray	**11** opt.
Mo−C(1)	1.83(1)	1.898	1.864(11)	1.898	1.879(7)	1.888
Mo−C(2)	2.05(1)	2.048	2.045(1)	2.054	2.057(7)	2.065
Mo−S(1)	2.529(2)	2.607	2.526(3)	2.603	2.504(1)	2.571
Mo−S(2)	2.547(2)	2.607	2.528(3)	2.602	2.497(2)	2.571
Mo−P(1)	2.435(2)	2.506	2.432(3)	2.502	2.419(2)	2.510
Mo−P(2)	2.430(3)	2.506	2.413(3)	2.498	2.411(1)	2.510
C(1)−Mo−C(2)	122.7(4)	125.9	120.1(4)	126.7	118.0(3)	124.4
S(1)−Mo−S(2)	69.9(8)	71.1	70.0(1)	71.5	71.9(1)	74.0
P(1)−Mo−P(2)	120.55(9)	116.9	119.7(1)	116.5	120.2(1)	117.4
S(1)−Mo−P(1)	154.80(9)	156.4	156.9(1)	156.8	155.4(1)	157.8
S(2)−Mo−P(2)	153.50(9)	156.4	152.7(1)	157.0	157.7(1)	157.8

[a] For the atom numbering, see Scheme 2. [b] Reference 6a. [c] Reference 6c.

Table 4. Relevant Bond Distances (Å) and Angles (deg) for the $Mo(COCH_2R)$ Fragment in Agostic Acyl Complexes[a]

	7[b] X-ray	**8** opt.	**2a-Me** X-ray	**9** opt.	**10**[c] X-ray	**11** opt.
Mo−C(2)	2.05(1)	2.048	2.045(11)	2.054	2.057(7)	2.065
Mo−C(3)	2.60(1)	2.613	2.69(11)	2.600	2.762(4)	2.671
Mo−Ha	2.06(9)	2.351	2.65(9)	2.247	2.56(6)	2.398
C(3)−Ha	1.00(9)	1.103	1.01(9)	1.108	1.00(9)	1.100
C(2)−C(3)	1.57(2)	1.595	1.587(15)	1.588	1.561(9)	1.585
Mo−C(2)−C(3)	90.9(8)	90.8	94.7(6)	90.2	98.6(4)	93.1
Mo−C(2)−O(2)	149.2(8)	147.5	148.1(8)	147.1	144.4(5)	145.7
C(3)−C(2)−O(2)	120(1)	121.7	117.2(9)	122.7	116.9(6)	121.2
C(2)−C(3)−Ha	99(5)	115.7	110(5)	114.1	116(5)	114.4

[a] For the atom numbering, see Scheme 2. [b] Reference 6a. [c] Reference 6c.

Scheme 2

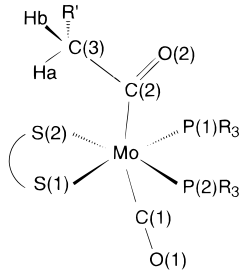

7 S,S = S_2CNMe_2, R=Me, R'=H

8 S,S = S_2CNH_2, R=H, R'=H

2a-Me S,S = S_2CNMe_2, R=Me, R'=$SiMe_3$

9 S,S = S_2CNH_2, R=H, R'=SiH_3

10 S,S = $S_2C(PMe_3)OCH_2CF_3$, R=Me, R'=H

11 S,S = $S_2C(PH_3)OH$, R=H, R'=H

$CO(PMe_3)_2$ (**2a-Me**), modeled as $Mo(C(O)CH_3)(S_2CNH_2)(CO)(PH_3)_2$ (**8**) and $Mo(C(O)CH_2SiH_3)(S_2CNH_2)(CO)(PH_3)_2$ (**9**), respectively. Additional calculations were also carried out on the phosphonium xanthate complex $Mo(C(O)CH_3)(S_2C(PMe_3)OCH_2CF_3)(CO)(PMe_3)_2$ (**10**)[6c] modeled as $Mo(C(O)CH_3)(S_2C(PH_3)OH)(CO)(PH_3)_2$ (**11**). Computed and experimental parameters concerning the coordination sphere of the metal are collected in Table 3, and those involved in the molybdenum-acyl interaction in Table 4. Atom numbering is shown in Scheme 2.

The data in Table 3 indicates a good agreement between the experimental and calculated geometrical parameters. Despite the simplifications introduced in the theoretical study, bond distances and bond angles are reproduced well by the calculations, with differences not larger than one tenth of an Ångstrom and six degrees, respectively, with respect the experimental values. The largest differences can be found for complex **11**, in which the most severe simplification of the experimental system **10** has been introduced, replacing the electron-drawing $-CH_2CF_3$ group by H. The modeling and computation process is therefore suitable for this system.

In the complexes under study, six ligands are coordinated to the metal. We will attempt to classify the geometry in terms of the most frequent polyhedron geometry found in transition metal: six-coordination.[12] Given that the three species adopt very similar geo-

(12) Kubacek, P.; Hoffmann, R. *J. Am. Chem. Soc.* **1981**, *103*, 4320.

Scheme 3

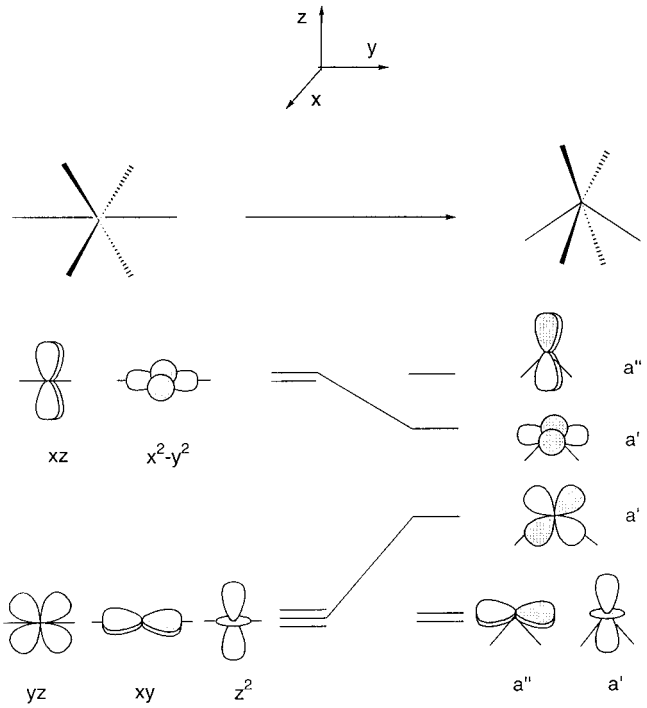

metrical arrangements, we will discuss only the (**2a-Me**) structure. In this complex the two S atoms and two P atoms define a plane, and the terminal carbonyl ligand and the agostic acyl ligand are in a plane perpendicular to that plane. The chelating dithiocarbamate ligand imposes a rigid angle (70.0° exp, 71.5° calcd). The S(1)−Mo-P(2) and S(2)−Mo-P(1) angles (83.0° exp, 85.7° calcd and 86.9° exp, 85.8° calcd respectively) are close to the ideal octahedral value (90°). However, the P(1)−Mo-P(2) (119.7° exp, 116.5° calcd) and more so the C(1)−Mo-C(2) (120.1° exp, 126.7° calcd) angles deviate substantially from those of the octahedron (90° and 180° respectively). We must recall our compounds are d^4-six-coordinate species and substantial deformations from octahedral geometry toward bicapped tetrahedron or trigonal prism geometry have been reported for these complexes.[12]

Actually **2a-Me** can be described as a distorted bicapped tetrahedron in which the two sulfur atoms of the xanthate and the carbon atoms of the acyl and carbonyl ligands occupy the tetrahedron vertexes whereas the two trimethyl phosphine ligands are the capping ligands that point toward two faces of the tetrahedron. The angles between the "tetrahedral" ligands are S(1)−Mo-C(1) = 108.0° exp, 101.1° calcd, S(1)−Mo-C(2) = 118.2° exp, 121.1° calcd, C(1)−Mo-C(2) = 120.1° exp, 126.7° calcd, and S(1)−Mo-S(2) = 70.0° exp, 71.5° calcd

A detailed theoretical analysis of the deformations from octahedral geometry in d^4 transition-metal complexes has been performed by Kubacek and Hoffmann.[12] The electronic consequences of the deformation from the octahedral geometry toward a bicapped tetrahedron can be understood with very simple orbital arguments.[13] In Scheme 3 we have traced a qualitative picture of the energetic evolution of the block-*d* orbitals along the geometric deformation. On the left side, there is the well-known orbital splitting for an octahedral ligand field. The three lower energy orbitals (d_{z^2}, d_{xy} and d_{yz}) are those oriented away from the ligands, while the two higher energy orbitals ($d_{x^2-y^2}$ and d_{xz}) point toward the ligands. When going toward the bicapped tetrahedron, the ligands initially in the *y*-axis are bent away toward negative values of the Z-coordinate. The $d_{x^2-y^2}$ orbital is stabilized because its two lobes directed along the *y*-axis are no longer pointing toward the two ligands. The energy of the d_{yz} orbital is increased because the two ligands that have moved are now pointing toward two lobes of this orbital. The d_{xy} and d_{xz} orbitals do not have contributions from the axial ligands, so they will not be affected by the distortion. The d_{z^2} orbital will be only slightly affected.

The resulting orbital energy scheme for the d set of orbitals of a bicapped tetrahedron complex consists of two low energy orbitals of different symmetry (a′ and a″ in the Cs group representation), two antibonding orbitals of the same symmetry (a′) and a highest a″ antibonding orbital. In a low-spin d^4 complex the two nonbonding orbitals are filled so this is a favorable electron-counting for the bicapped tetrahedral structure.

The most noteworthy feature of complexes **2a-Me**, **7**, and **10** is the strong distortion of the metal-acyl fragment with respect to the geometry expected for a monohaptoacyl coordination. This distortion, mainly reflected in the values of the Mo−C(2)−C(3) angles, causes a pivoting of the CH_2R group of the acyl ligand toward the metal. As can be seen in Table 4, the agostic distortion is also found in the optimized geometries of the model complexes **8**, **9**, and **11**. Optimized geometric parameters of the Mo-acyl fragment agree well with the X-ray determined values.[6] The largest differences are found for the Mo−H distance, but this could be explained by the uncertainty in the X-ray determination of H atoms. Although the calculations resolve *β*-agostic structures as the most stable of the three systems considered, they are not able to reproduce the experimental differences between **7**, **2a-Me**, and **10**. The Mo−C(2)−C(3) angle of **8** (90.8°) is in excellent accord with the experimental value of **7** (90.9°).[6a] However, the increase of ca. 5° of this angle, due to the substitution of a H atom of the acyl CH_2R group by $SiMe_3$, is not found in model system **9**. There is also a difference for the Mo−C(1)−C(3) angle of 5° between **10** and **11.** The results indicate that the very subtle electronic differences introduced in the experimental systems by changing groups in the S−S donor ligand or the R of the acyl ligand are not accounted for by the model systems.

The origin of the agostic distortion observed in the Mo-acyl complexes can be understood with the help of the qualitative orbital picture presented in Scheme 3. These species are d^4-Mo(II) compounds with a formal valence electron count for Mo of 16. The two occupied d orbitals are d_{z^2} and d_{xy}. The bonding of the monohapto C_{acyl} to the metal is mainly due to the interaction of the C_{acyl} lone pair with a lobe of the d_{yz} orbital. The agostic distortion allows the involvement of the $d_{x^2-y^2}$ orbital in the M−C_{acyl} bond. Both d_{yz} and $d_{x^2-y^2}$ are a′ orbitals and mix to reinforce the M−C_{acyl} bond. The agostic distortion brings the C(3) and H(2) atoms of the acyl fragment close to the molybdenum atom, where they can

(13) Albright, T. A.; Burdett, J. K.; Whangbo, M. H. *Orbital Interactions in Chemistry*; Wiley: New York, 1985; pp 289−294.

Scheme 4

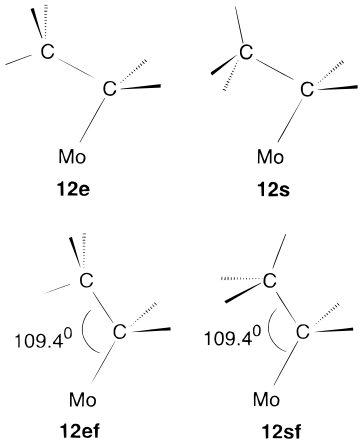

interact with the $4d_{x^2-y^2}$, 5s and $5p_y$ metal orbitals, all of them empty. Thus, an agostic interaction between the metal and the $-CH_2R$ group of the acyl ligand is at work in these systems. In what follows we will analyze in detail this interaction, focusing on the $Mo(COCH_3)(S_2CNH_2)(CO)(PH_3)_2$ system **8**.

Theoretical Analysis of the *β*-Agostic Interaction. To our knowledge, the only agostic acyl compounds experimentally characterized are the series of molybdenum complexes $Mo(COCH_2R)(S_2CX)(CO)(PMe_3)_2$. Several *β*-agostic ethyl complexes have been reported,[2] and they are experimental and theoretical benchmarks for ethyl *β*-agostic interactions.[14] To go further into the analysis of the specificity of the agostic interaction in acyl complexes we have also analyzed theoretically the interaction of an $Mo(S_2CX)(CO)(PR_3)_2$ metal fragment with an ethyl ligand. Given the electronic structure of this d^4-metal fragment, it may be hoped that it will also develop a *β*-agostic interaction with the ethyl. In this way, we will be able to compare acyl and ethyl *β*-agostic interactions.

To better analyze this interaction, we performed for complex **12** a series of geometry optimizations with different constraints. These geometries are shown in Scheme 4. The first of them, corresponding to the absolute minimum, has no constraints, and has the $C_\beta-H$ bond eclipsed with respect to the $Mo-C_\alpha$ bond. It is labeled **12e**. A second geometry optimization, **12s**, was performed with a forced staggered conformation around the $C_\alpha-C_\beta$ bond. Both **12e** and **12s** present an important agostic distortion, with values of the $Mo-C_\alpha-C_\beta$ angle of 84.8° and 86.6°, respectively. Two other geometry optimizations, **12ef** and **12sf**, were carried out with an anagostic arrangement. This was accomplished through freezing the $Mo-C_\alpha-C_\beta$ angle to a tetrahedral value of 109.4°. The relative energies of these four structures, together with the geometric parameters that describe the ethyl coordination, are collected in Table 5. The optimized geometry of the most stable structure **12e** is presented in Figure 3.

12e is the minimum energy structure for **12**, indicating that a $Mo(S_2CX)(CO)(PR_3)_2$ metal fragment should establish a *β*-agostic interaction with an ethyl ligand. Besides the distorted $Mo-C_\alpha-C_\beta$ angles, the $C_\beta-H$ bond that points to the metal is significantly lengthened (1.127 Å vs 1.10 Å for a normal C−H bond). Moreover, geometric parameters for the metal-ethyl fragment in **12e** are very similar to those of the well characterized *β*-agostic $EtTiCl_3$(dmpe) complex.[14] In particular, the $Mo-C_\alpha-C_\beta$ angle is very close to the $Ti-C_\alpha-C_\beta$ angle (86.3(6)° X-ray, 293 K,[14a] 84.57(9)° X-ray, 105 K[14d]). Optimization of **12** with a staggered ethyl group (species **12s**) gives also an agostic conformer, characterized by a $Mo-C_\alpha-C_\beta$ angle of 92.3°. This conformer is calculated to lie only 2.4 kcal mol^{-1} above the minimum structure **12e**. As it has been shown very recently in a thorough study of *β*-agostic interactions, these interactions do not necessarily require an ethyl group in which a $C\beta-H$ bond points toward the metal atom.[14d] In **12s** all the $C_\beta-H$ bond distances have the same value, pointing to the absence of a direct M−H interaction. In agreement with the theoretical study of $EtTiCl_3$(dmpe),[14d] methyl rotation occurs in **12** with only a small change of the Mo−C−C angle. Early EH calculations in the agostic $[Co(C_5Me_5)(Et)(PMe_2Ph)]^+$ complex indicated a different mechanism for the methyl rotation, in which the rotation about the $C_\alpha-C_\beta$ bond takes place after cleavage of the agostic interaction.[15]

The anagostic structures **12ef** and **12sf** are not minima in the potential energy surface and have considerably higher energies than **12e**: 11.3 kcal mol^{-1} for the eclipsed **12ef** and 9.3 kcal mol^{-1} the staggered **12sf**. The energy of the agostic interaction in **12** is in the range of the interaction energies determined in experimental[16] and computational[17] studies of agostic

Table 5. Optimized Geometrical Parameters (Å and deg) for the Metal−Ethyl Fragment in $Mo(CH_2CH_3)(S_2CNH_2)(CO)(PH_3)_2$ (12)

	12e	12s	12ef	12sf
Mo−C(2)	2.243	2.249	2.246	2.260
Mo−C(3)	2.605	2.654	3.130	3.136
Mo−Ha[a]	2.168	2.683	2.950	3.284
C(3)−Ha[a]	1.127	1.104	1.108	1.101
C(3)−Hb	1.098	1.102	1.098	1.102
C(2)−C(3)	1.546	1.548	1.558	1.550
C(2)−H(2)	1.094	1.095	1.097	1.098
Mo−C(2)−C(3)	84.8	86.6	109.4[b]	109.4[b]
Mo−C(2)−H(2)	118.1	118.4	112.8	113.1
H(2)−C(2)−C(3)	112.7	111.6	108.6	107.9
C(2)−C(3)−Ha	114.1	111.9	113.0	111.9
C(2)−C(3)−Hb	112.0	111.2	110.9	109.5
rel energy[c]	0.0	2.4	11.3	9.3

[a] Ha refers to the hydrogen atom closest to the metal. [b] Fixed value. [c] In kcal mol^{-1}.

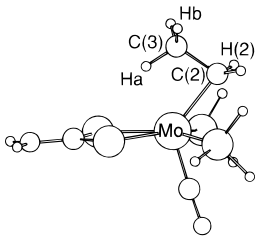

Figure 3. Optimized geometry of the most stable structure of $Mo(CH_2CH_3)(S_2CNH_2)(CO)(PH_3)_2$ (**12e**).

(14) (a) Dawoodi, Z.; Green, M. L. H.; Mtetwa, V. S. B.; Prout, K.; Schult, A. J.; Williams, J. M.; Koetzle, T. F. *J. Chem. Soc., Dalton Trans.* **1986**, 1629. (b) McGrady, G. S.; Downs, A. J.; Haaland, A.; Scherer, W.; Mckean, D. C. *Chem. Commun.* **1997**, 1547. (c) Popelier, P. L. A.; Logothetis, G. *J. Organomet. Chem.* **1998**, *555*, 101. (d) Haaland, A.; Scherer, W.; Rund, K.; McGrady, G. S.; Downs, A. J.; Swang, O. *J. Am. Chem. Soc.* **1998**, *120*, 3762.

(15) Cracknell, R. B.; Orpen, A. G.; Spencer, J. L. *J. Chem. Soc, Chem. Commun.* **1986**, 1005.

systems (10−15 kcal mol^{-1}). The pivoting of the methyl group toward the metal causes a notable stabilization of the system. The agostic interaction has been often thought as the result of the electronic donation from a C−H bond to a metal low-lying vacant orbital, to fill a vacant coordination site in an electron deficient compound.[2,18] There are however a growing number of experimental and theoretical studies pointing to the need for a more elaborate analysis of agostic interactions. On one hand, it has been recently proved that in some systems steric effects of bulky phosphines can assist in stabilizing agostic interactions.[19] On the other hand, a theoretical study of β-agostic interactions in titanium ethyl derivatives has shown that the agostic distortion takes place regardless of the orientation of the C−H bond. Following that analysis, one can divide the agostic interaction into two terms, corresponding to the M−H and M−C$_\beta$ interaction. From our calculations it is possible to roughly separate the two contributions in complex **12**. The energy difference between the two eclipsed conformations (11.3 kcal mol^{-1}) gives the total energy of the β-agostic interaction, whereas the energy difference between the two staggered conformations (6.9 kcal mol^{-1}) approximates the Mo−C$_\beta$ contribution. Thus, the direct M−H component of the agostic interaction in **12** can be estimated as 4.4 kcal mol^{-1}. This component is enough to invert the relative stabilities of the eclipsed and staggered conformations with respect to the anagostic situation. All these energy values agree with the presence of a strong β-agostic interaction between the methyl group of the ethyl ligand and the metal fragment in **12**, even stronger than in TiEtCl$_3$(dmpe). For instance, Becke3LYP calculations in the titanium complex have produced staggered agostic and anagostic structures at 0.2 and 1.8 kcal mol^{-1} respectively, above the eclipsed agostic minimum.[14c] A value of 8.4 kcal mol^{-1} has been calculated for the β-agostic stabilization energy of the model [EtTiCl$_2$]$^+$ cation.[14c]

The well-known sensitivity of MP2 results to the basis set could cast some doubt on the validity of our quantitative analysis, in particular because we are dealing with weak interactions. To evaluate the basis set dependence of the results, the energy of some selected points was recomputed in the same frozen geometry with a much larger basis set (basis set II) which included polarization functions in all atoms. The energies recomputed in this way were those of the agostic structures **12e** and **12s**, and those of the anagostic structures **12ef** and **12sf**. Changes were minimal. The relative energies, which were 0.0, 2.4, 11.3, and 9.3 kcal/mol with basis set I, became 0.0, 2.4, 13.1, and 11.0 kcal/mol with the more extended basis set II. The agostic structures **12e** and **12s** have exactly the same energy difference, and the anagostic species are destabilized by ca. 2 kcal/mol with respect to the agostic ones. These values would give an estimation of 8.6 kcal/mol for the Mo−C$_\beta$ component of the agostic stabilization and 4.5 kcal/mol for the Mo−H component. In summary, these frozen geometry calculations prove that basis set I provides a sufficiently accurate picture.

We have repeated the same calculations presented in the previous paragraph for the ethyl complex **12** in the case of the acyl complex **8**. In this way, in addition to the most stable conformation for the Mo(C(O)CH$_3$)(S$_2$CNH$_2$)(CO)(PH$_3$)$_2$ system, in which the C$_\beta$−H bond eclipses the M−C$_\alpha$ bond (from now on **8e**), we have also optimized **8** with staggered acyl (**8s**), and avoiding the β-agostic interaction by fixing the Mo−C$_\alpha$-C$_\beta$ angle at 120° with an eclipsed (**8ef**) and staggered (**8sf**) acyl conformations (see Scheme 5). Geometric parameters describing the metal-acyl fragment in the four structures, together with their relatives energies, are collected in Table 6. The optimized geometries of the most stable structure are pictured in Figure 4.

At first glance, results for **8** and **12** are very similar. In the most stable conformation of both a very acute Mo−C$_\alpha$−C$_\beta$ angle is found and a C$_\beta$−H bond of the

Table 6. Geometrical Parameters (Å and deg) for the Metal−Acyl fragment in Mo(CH$_3$CO)(S$_2$CNH$_2$)(CO)(PH$_3$)$_2$ (8)

	8e	8s	8ef	8sf
Mo−C(2)	2.048	2.044	2.106	2.128
Mo−C(3)	2.613	2.661	3.180	3.198
Mo−Ha[a]	2.351	2.800	3.158	3.406
C(3)−Ha	1.103	1.098	1.100	1.101
C(3)−Hb	1.097	1.097	1.098	1.097
C(2)−C(3)	1.595	1.623	1.552	1.549
C(2)−O(2)	1.248	1.248	1.276	1.275
Mo−C(2)−C(3)	90.8	92.3	120.0[b]	120.0[b]
Mo−C(2)−O(2)	147.5	146.7	126.7	125.6
O(2)−C(2)−C(3)	121.7	121.0	113.3	114.4
C(2)−C(3)−Ha	115.7	113.4	113.9	111.1
C(2)−C(3)−Hb	107.4	101.7	107.8	107.1
rel energy[c]	0.0	4.0	12.7	13.8

[a] Ha refers to the hydrogen atom closest to the metal. [b] Fixed value. [c] In kcal mol^{-1}.

Scheme 5

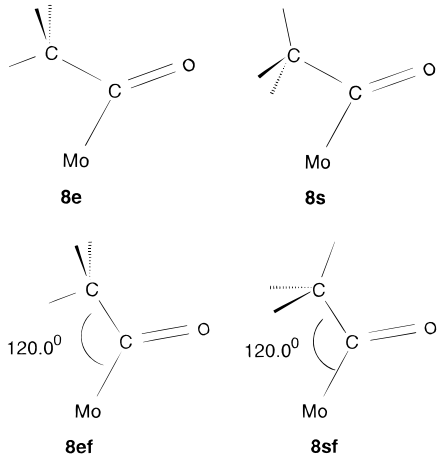

(16) (a) Crabtree, R. H. *Chem. Rev.* **1985**, *85*, 245. (b) González, A. A.; Zhang, K.; Nolan, S. P.; López de la Vega, R.; Mukerjee, S. L.; Hoff, C. D.; Kubas, G. L. *Organometallics* **1988**, *7*, 2429. (c) Burger, B. J.; Thompson, M. E.; Cotter, W. D.; Bercaw, J. E. *J. Am. Chem. Soc.* **1990**, *112*, 1566. (d) Zhang, K.; González, A. A.; Mukerjee, S. L.; Chou, S.-J.; Hoff, C. D.; Kubat-Martin, K. A.; Barnhart, D.; Kubas, G. J. *J. Am. Chem. Soc.* **1991**, *113*, 9170.

(17) (a) Kawamura-Kuribayashi, H.; Koga, N.; Morokuma, K. *J. Am. Chem. Soc.* **1992**, *114*, 2359. (b) Lohrenz, J. C. W.; Woo, T. K.; Ziegler, T. *J. Am. Chem. Soc.* **1995**, *117*, 12793. (c) Margl, P.; Lohrenz, J. C. W.; Ziegler, T.; Blöchl, P. E. *J. Am. Chem. Soc.* **1996**, *118*, 4434. (d) Thomas, J. L. C.; Hall, M. B. *Organometallics* **1997**, *16*, 2318. (e) Musaev, D. G.; Froese, R. D. J.; Svensson, M.; Morokuma, K. *J. Am. Chem. Soc.* **1997**, *119*, 367. (f) Han, Y.; Deng, L.; Ziegler, T. *J. Am. Chem. Soc.* **1997**, *119*, 5939. (g) Deng, L.; Woo, T. K.; Cavallo, L.; Margl, R. M.; Ziegler, T. *J. Am. Chem. Soc.* **1997**, *119*, 6177.

(18) (a) Crabtree, R. H. *Angew. Chem., Int. Ed. Engl.* **1993**, *32*, 789. (b) Shilov, A. E.; Shul'pin, G. B. *Chem. Rev.* **1997**, *97*, 2879.

(19) Ujaque, G.; Cooper, A. C.; Maseras, F.; Eisenstein, O.; Caulton, K. G. *J. Am. Chem. Soc.* **1998**, *120*, 361.

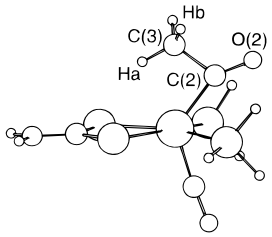

Figure 4. Optimized geometry of the most stable structure of $Mo(COCH_3)(S_2CNH_2)(CO)(PH_3)_2$ (**8e**).

terminal methyl eclipses the $M-C_\alpha$ bond. Thus, an agostic interaction is taking place. In both the ethyl and acetyl derivatives the agostic distortion is still present in the staggered conformation ($Mo-C_\alpha-C_\beta$ angles of 86.6° and 92.3° in **12s** and **8s**, respectively). Clearly, there is no need of a direct M−H interaction for the agostic distortion to take place. In **8** and **12**, methyl rotation occurs with a low energy barrier and with only a small variation of the $Mo-C_\alpha-C_\beta$ angle. The energetic gain associated with the distortion is also similar (around 12 kcal mol^{-1}). However, a more detailed inspection of the data shows important differences between **8** and **12**. The separation of the M−H and Mo − C_β contributions to the agostic stabilization of **8e** (12.7 kcal mol^{-1}) gives an estimation of 9.8 kcal mol^{-1} for the Mo − C_β component and only 2.9 kcal mol^{-1} for the M−H component. The Mo···C_β bonding plays a more important role in stabilizing the *β*-agostic acyl than it does in the ethyl derivative. The stability of the results on complex **8** with respect to extension of the basis set was again tested with single point calculations on basis set II. Changes were again very small. The relative energies of **8e**, **8s**, **8ef**, and **8sf** with basis set II were 0.0, 4.3, 15.9, and 17.0 kcal mol^{-1}, while 0.0, 4.0, 12.7, and 13.8 kcal mol^{-1} values were obtained with basis set I. The agostic stabilization obtained from these frozen geometry calculations would be of 15.9 kcal mol^{-1} for **8e**, with contributions of 12.7 and 3.2 kcal mol^{-1} from the $Mo-C_\beta$ and Mo−H components, respectively.

Geometric parameters of the agostic structures of **8** are in accord with this behavior. In contrast to what is found in **12**, in **8e** there is not a significant increase of the in-plane $C_\beta-H$ bond distance. On the contrary, a remarkable lengthening of the $C_\alpha-C_\beta$ bond distance occurs in **8e** and **8s**. This fact can be seen by comparing the $C_\alpha-C_\beta$ distance in agostic and anagostic eclipsed structures (1.595 and 1.552 Å, respectively). The value in **8ef** is very similar to that determined by X-ray diffraction in the monohaptoacyl complex $CpMo(COCH_3)(CO)_2(PPh_3)$ (1.555 Å), in which a normal $Mo-C_\alpha-C_\beta$ angle of 120.9 ° was found.[11] To ensure that the interaction $Mo-C_\beta$ is responsible for the increase of the C−C distance, we have also optimized the species CH_3CONa, with a fixed Na−C−O angle of 120°. A value of 1.563 Å was obtained for the C−C distance, confirming that our methodology furnishes acyl C−C distances not longer than 1.56 Å when a metal − C_β interaction is not present. A similar stretching of C−C bonds has been found in several theoretical studies[17a,17b,20] and in a very recent X-ray diffraction study.[21] In all cases stretching has been interpreted in terms of C−C agostic interaction. Interestingly, the variation of the $C_\alpha-C_\beta$ distance between **12e** and **12ef**, although slight, is in the opposite direction. A small reduction of the C−C bond distance is obtained in going from the anagostic to the agostic structures (from 1.558 to 1.546 Å).

It is also worth mention that the $Mo-C_\alpha$ bond distance is shortened in forming the agostic interaction. Although this trend is observed in both the ethyl and acetyl derivatives, it becomes much more pronounced in the agostic acyl. This fact has also been proved in agostic alkylidene transition metal complexes,[22] and has been interpreted from extended Hückel by saying that the strengthening of the $Mo-C_\alpha$ bond is the driving force for the α-agostic distortion.[23] It must be remarked that in **8** the strengthening of the $Mo-C_\alpha$ bond and the weakening of the $C_\alpha-C_\beta$ in the agostic structures are also coupled with a remarkable shortening of the acyl CO distance (from 1.270 Å in **8ef** to 1.248 Å in **8e**).

Our theoretical studies on the acetyl complex indicate an important activation of the $C_\alpha-C_\beta$ in the agostic structures. To determine if the activation is a consequence of the presence of the agostic methyl group in the acyl ligand or whether it is a more general phenomenon, we have also considered the same dithiocarbamate metal fragment but now with a formyl ligand. The optimized geometry of the $Mo(HCO)(S_2CNH_2)(CO)(PH_3)_2$ model complex is similar to that found for the acetyl compound. A strong agostic distortion is taking place in the formyl system, reflected in the very acute $Mo-C_\alpha-H_\alpha$ angle (65.6°). Other remarkable geometrical parameters are the $C_\alpha-H$, $Mo-C_\alpha$, and acyl C−O bond distances of 1.336, 1.937, and 1.334 Å, respectively. All these values, together with the $Mo-H_\alpha$ distance of 1.844 Å suggest that the structure we have obtained is along the path of the migratory CO insertion reaction.

Comparison between ethyl and acyl *β*-agostic molybdenum complexes has shown that, despite the similar structural features they present, there is an important difference between them. Whereas the agostic ethyl complex can be considered as an arrested structure on an initial step of the reaction path corresponding to *β*-elimination, the agostic acetyl complex can be seen as an arrested point in the CO insertion reaction into the Mo−C bond. In the next section we will further analyze this aspect.

Migratory CO Deinsertion Reaction. Our experimental results[6,9a,28] indicate that molybdenum and tungsten acyl complexes $M(COCH_2R)(S_2CX)CO(PMe_3)_2$ can easily undergo CO deinsertion to produce the seven coordinate alkyl-carbonyl isomers $M(CH_2R)(S_2CX)(CO)_2(PMe_3)_2$. In addition, we have shown in the preceding

(20) Koga, N.; Morokuma, K. *J. Am. Chem. Soc.* **1988**, *110*, 108.
(21) Tomaszewski, R.; Hyla-Kryspin, I.; Mayre, C. L.; Arif, A. M.; Gleiter, R.; Ernst, R. D. *J. Am. Chem. Soc.* **1998**, *120*, 2959.
(22) Schultz, A. J.; Brown, R. K.; Williams, J. W.; Schrock, R. R. *J. Am. Chem. Soc.* **1981**, *103*, 169.
(23) (a) Goddard, R. J.; Hoffmann, R.; Jemmis, E. D. *J. Am. Chem. Soc.* **1980**, *102*, 7667. (b) Eisenstein, O.; Jean, Y. *J. Am. Chem. Soc.* **1985**, *107*, 1177. (c) Demolliens, A.; Jean, Y.; Eisenstein, O. *Organometallics* **1986**, *5*, 1457.
(24) Maseras, F.; Eisenstein, O. *New J. Chem.* **1997**, *21*, 961.
(25) Versluis, L.; Ziegler, T. *Organometallics* **1990**, *9*, 2985.
(26) Curtis, M. D.; Shiu, K. B.; Butler, W. M. *J. Am. Chem. Soc.* **1986**, *108*, 1550.
(27) (a) Herrick, R. S.; Templeton, J. L. *Inorg. Chem.* **1986**, *25*, 1270. (b) Kellner, R.; Prokopwoski, P.; Malissa, H. *Anal. Chim. Acta* **1974**, *68*, 401.
(28) Strong influence of steric effects has been found to favor six-coordinated dihaptoacyl coordination over the seven-coordinated alkyl-carbonyl formulation in related tungsten compounds: see ref 30.

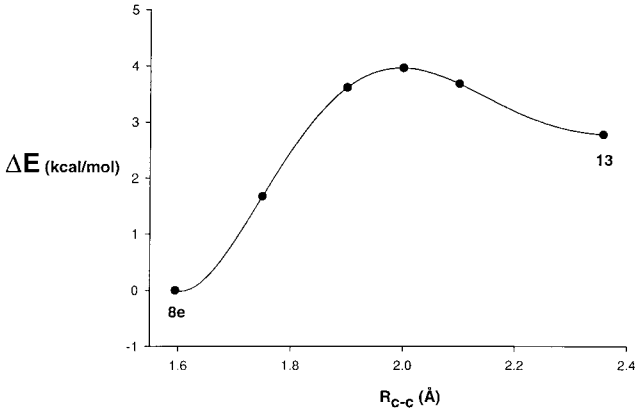

Figure 5. Energy profile for the lengthening of the C−C distance in the complex $Mo(COCH_3)(S_2CNH_2)(CO)(PH_3)_2$ (**8e**).

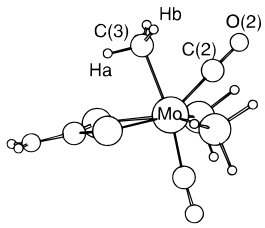

Figure 6. Optimized geometry of the $Mo(CH_3)(S_2CNH_2)(CO)_2(PH_3)_2$ (**13**) complex.

section that an important lengthening of the acyl C−C bond is associated to the agostic distortion. To establish the relationship between such a distortion and the C−C bond breaking process we have studied theoretically the reaction path for the interconversion between the β-agostic acyl and the alkyl-carbonyl isomers of **8**.

Starting from the minimum **8e**, we have calculated the energy profile for the CO deinsertion by optimizing the geometry of the system at several fixed values of the C−C distance. The potential energy curve obtained is presented in Figure 5. A maximum is reached at C−C = 2.0 Å. Full geometric optimization starting at the geometry with C−C = 2.1 Å leads to a stable seven-coordinate species **13** with a methyl carbonyl nature (C···C = 2.357 Å, see Figure 6).

Inspection of the geometric changes along the reaction coordinate shows that, as expected, the $C_\alpha-C_\beta$ lengthening is accompanied by $C_\alpha O$ shortening, $Mo-C_\beta$ shortening, and closure of the $Mo-C_\alpha-C_\beta$ angle. Only the geometric parameters of the metal−acyl fragment change appreciably; the rearrangement of the other ligands in the coordination sphere of the metal is only minor. In the methyl-carbonyl structure the $Mo-C_\alpha$ and $Mo-C_\beta$ distances have values of 1.932 and 2.390 Å, respectively, and the $Mo-C_\alpha-C_\beta$ angle has closed to 66.9°. The seven-coordinate species is better described[24] as a capped octahedron, with the carbonyl $C_\alpha O$ group as capping ligand, although quite distorted because of the presence of the chelating xanthate ligand (Figure 6). We note that other heptacoordinate species may be attainable with a low energy barrier for the interconversion. We have limited the study of the methyl-carbonyl derivatives to the one directly reached by the breaking of the acyl C−C bond in the conformation it has in the minimum energy structure.

The most remarkable result of this calculation is the extremely low energy barrier (4.0 kcal mol^{-1}) found for the C−C bond breaking process in the molybdenum acyl complex **8**. Moreover, the alkyl-carbonyl structure **13** lies only 2.8 kcal mol^{-1} above the acyl isomer. Hence, the reverse reaction, the migratory CO insertion, takes place with an energy barrier of only 1.2 kcal mol^{-1}. This value is much lower than those previously calculated for the migratory CO insertion in $Rh(PH_3)_2Cl(H)(CH_3)(CO)$ (27.4 kcal mol^{-1})[8] and in $CH_3Mn(CO)_5$ (18 kcal mol^{-1}).[25] The energy barriers for the C−C bond forming and breaking processes in **8** are of the same order as those of the methyl rotation. Interestingly, this result is fully consistent with our previous experimental observation of a fluxional behavior of $Mo(\overline{C(O)CH_3})(S_2CNMe_2)CO(PMe_3)_2$ leading to the equivalence of the two carbonyl groups. This process is also likely to go through a 7-coordinate methyl species, and its free energy of activation was estimated to be 9.4 kcal mol^{-1}. The difference between this value and the 4.0 kcal mol^{-1} computed here is likely associated with the fact that **8e** does not seem the most appropriate isomer for the fluxionality process, which probably requires more severe rearrangements and the involvement of higher energy 7-coordinate isomers. For comparative purposes, we have also computed the energy profile for the β-elimination in **8**. In this case the C_β-H bond is broken. Optimization of several points at fixed values of the C_β-H distances gives a monotonic energy rise: 9.0 kcal mol^{-1} at C_β-H = 1.30 Å, 25.7 kcal mol^{-1} at C_β-H = 1.50 Å, 42.5 kcal mol^{-1} at C_β-H = 1.75 Å, and 46.3 kcal mol^{-1} at C_β-H = 1.90 Å. There is no minimum for the system in this direction.

It is clear that the β-agostic interaction between the terminal methyl group of the acyl ligand and the metal is able to stabilize a very advanced structure in the reaction path that leads to the alkyl-carbonyl species. Furthermore, this interaction assists the C−C bond breaking process. The small energy difference between the acyl and alkyl-carbonyl isomers of **8** justifies the explanation that subtle changes in the basicity of the metal, or in the donating ability or the steric requirements of the ancillary ligands, could significantly shift the acyl/alkyl-carbonyl equilibrium.

Solution Behavior of Compounds 2−6. Multinuclear (^1H, $^{13}C\{^1H\}$ and $^{31}P\{^1H\}$) NMR studies of solutions prepared from crystalline samples of **2a-Me** or **2a-Ph** in $C_6D_5CD_3$, C_6D_6, or CD_2Cl_2 clearly show the existence of two sets of resonances. By comparison with the data already available for dihapto and agostic acyls of composition $Mo(C(O)CH_3)(S_2CX)CO(PMe_3)_2$,[6] the spectra can unequivocally be assigned to a mixture of the two complexes, that is, the agostic $Mo(\overline{C(O)CH_2SiMe_2R})(S_2CNMe_2)CO(PMe_3)_2$ (R = Me, **2a-Me**; Ph, **2a-Ph**) and the dihapto $Mo(\eta^2\text{-}C(O)CH_2SiMe_2R)(S_2CNMe_2)CO(PMe_3)_2$ (R = Me, **2d-Me**; Ph, **2d-Ph**) isomers, the latter being predominant. In the previously mentioned solvents the **2d**/**2a** ratio does not change appreciably, either with time or temperature, once the values of 6.6 (R = Me) and 3.4 (R = Ph) are attained. The agostic-to-dihapto acyl isomerization is favorable even at low temperatures. Thus when a crystalline sample of **2a-Me** is dissolved at −40 °C and the NMR spectra are recorded at that temperature, a **2d**/**2a**-Me ratio of ca. 1 is observed and this value quickly increases to ca. 6

Scheme 6

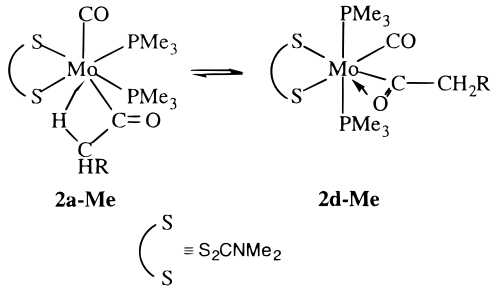

Scheme 7

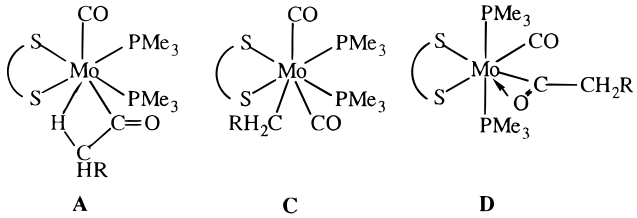

upon warming to room temperature. Further cooling of the mixture does not cause any observable variation. Interestingly, an identical isomeric composition is obtained when a crystalline sample of **2d-Me** is dissolved. It seems therefore clear that the agostic acyls **2a** readily evolve in solution to their dihaptoacyl isomers **2d** until equilibrium is achieved (Scheme 6). This behavior parallels prior observations for the acetyl compounds $Mo(C(O)CH_3)(S_2COR')CO(PMe_3)_2$ (R′ = Me, Et, *i*-Pr) which crystallize as the agostic form but exist in solution mostly as mixtures of the **A** and **D** structures (Scheme 7). As opposed to the behavior of complexes **2**, compound **3** exists in solution predominantly as the dihapto isomer, with only minor signals due to the β agostic species.

In contrast with their acetyl-dithiocarbamate counterparts, the xanthate compounds **5** and **6** occur in solution in the form of the dihaptoacyl isomer only. The same applies to the pyrrolyl dithiocarbamate derivative **4**. It is worth mentioning at this point that the dihaptoacyls **2d**−**6d** display dynamic properties in solution. For example, the two ^{31}P nuclei of complex **2a-Me** appear at −90 °C as an AB spin system with $^2J_{PP}$ = 115 Hz. This pattern of lines coallesces upon warming and finally gives a singlet at room temperature. As described previously, this fluxional behavior is due to a libration motion of the η^2-acyl moiety, which creates an effective plane of symmetry.[26]

With regard to the relative stability of the isomeric acyl structures, the silyl derivatives **2**−**6** follow the trend already described for the corresponding acetyl complexes (R = H). For the latter compounds, strongly donating chelating ligands favor the agostic coordination, whereas less electron-releasing ligands enhance the dihapto structure. Thus, in our case the dimethyl dithiocarbamate derivatives **2** exist in solution as isomeric mixtures, while the complex **4d-Me**, which contains the less donating pyrrol dithiocarbamate,[27] occurs in solution exclusively as the dihapto isomer.

The availability of the silyl derivatives **2**−**6** allows the further establishment of a sequence of reactivity concerning the tendency of compounds of composition $Mo(C(O)CH_2R)(S_2CNMe_2)CO(PMe_3)_2$ to undergo exchange

Scheme 8

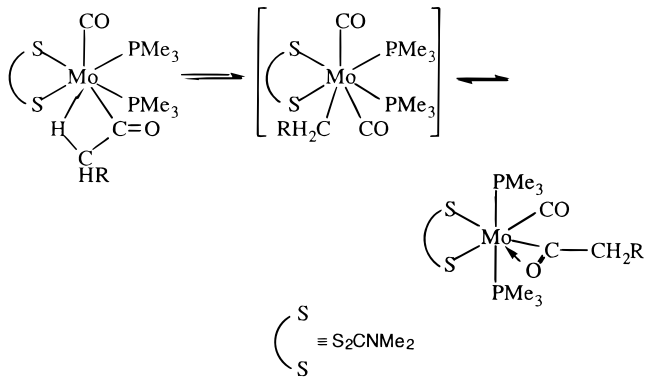

between the isomeric agostic acyl (**A**), dihaptoacyl (**D**), and alkyl carbonyl (**C**) structures (Scheme 7). The molybdenum acyl complex $Mo(C(O)CH_2CMe_3)(S_2CNMe_2)CO(PMe_3)_2$ derived from the neopentyl group, i.e., with R = CMe_3, exists only as the dihapto isomer, while the corresponding acetyl derivative (R = H) occurs as the agostic complex. In this case, however, variable temperature NMR studies have shown[9b,c] that the two degenerate ground-state structures possible for this compound (and its analogues) interconvert rapidly at room temperature through the undetected alkyl(carbonyl) isomer **C**. When R = $SiMe_3$, an intermediate situation is found because, as described above, the solutions of these complexes contain mixtures of the agostic and the dihapto acyl isomers. These differences appear to be mostly steric in origin.[28]

Some final comments will be devoted to the interconversion of structures of type **A** and **D**. Obviously, the proposed mechanism should take into account the different stereochemistry of the two isomers. Thus, simple releasing of the β-CH interaction and recoordination of the acyl through the oxygen atom would not be satisfactory. As mentioned both throughout this article and in previous publications[6,9a,29] molybdenum and tungsten acyl complexes of composition $M(C(O)CH_2R)(S_2CX)CO(PMe_3)_2$ can readily undergo deinsertion to produce the corresponding seven-coordinate alkylcarbonyl isomers $M(CH_2R)(L-L)(CO)_2(PMe_3)_2$. Since seven-coordinate species can easily undergo ligand rearrangements, a plausible mechanism for the isomerization process could involve CO deinsertion from the agostic complexes to give the corresponding alkylcarbonyls, followed by ligand redistribution and subsequent CO insertion to generate the dihaptoacyl compounds with their preferred stereochemistry (Scheme 8). Similar seven-coordinate intermediates have been proposed for the irreversible transformation of $[Mo](\eta^2\text{-}C(O)R)(CNR')$ complexes into their isomeric dihaptoiminoacyl-carbonyl compounds $[Mo](\eta^2\text{-}C(NR')R)(CO)$.[29] In addition we have demonstrated that tungsten alkyls of composition $W(CH_2R)(S_2CNMe_2)(CO)_2PMe_3$ show fluxional behavior at room temperature due to ligand mobility around the coordination sphere of the metal.[30]

Conclusions

Small energy differences have been observed between the agostic and the dihapto coordination modes of the

(29) Pizzano, A.; Sánchez, L.; Altmann, M.; Monge, A.; Ruiz, C.; Carmona, E. *J. Am. Chem. Soc.* **1995**, *117*, 1759.

(30) Carmona, E.; Contreras, L.; Poveda, M. L.; Sánchez, L. J.; Atwood, J. L.; Rogers, R. D. *Organometallics* **1991**, *10*, 61.

acyl ligand in $Mo(C(O)CH_2SiMe_2R)(S_2CX)(CO)(PMe_3)_2$ complexes. As previously observed in the analogous acetyl derivatives, strongly electron-releasing ligands appear to favor the agostic interaction, but the preference is not very pronounced; small changes in the steric effects around the metal, or in the nature of the co-ligands, can unbalance the situation in favor of any of the two isomers.

Ab initio calculations show that the agostic interaction between the acyl ligand and the Mo atom observed in the $Mo(C(O)CH_2R)(S_2CNH_2)(CO(PH_3)_2$ models is significant and lie well in the range observed for other $M-H-C_\beta$ nonclassical interactions that exist in metal alkyls. Separation between the M−H and $M-C_\beta$ contributions indicates a stronger importance of the latter (9.8 vs 2.9 kcal mol^{-1}), thus allowing the rotation around the C_α-C_β bond without cleavage of the agostic interaction. By comparison with the monohapto situation, the interaction between the $C(O)CH_3$ fragment and the metal center brings the Mo and C_β atoms closer, shortens the C−O and $Mo-C_\alpha$ bonds, and lengthens the $C_\alpha-C_\beta$ bond. This scenario can be viewed as an advanced intermediate along the reaction path of the CO deinsertion process in a monohapto acyl. An energy profile of the agostic acyl to the alkyl-carbonyl carried out by optimization of the molecular geometries at different C_α-C_β bond distances indicates a low energy barrier for the deinsertion process, in excellent accord with the behavior observed in solution for the $Mo(C(O)CH_3)(S_2CX)CO(PMe_3)_2$ complexes.

Experimental Section

Microanalyses were carried out either by the Analytical Service of the University of Seville or by Pascher Microanalytical Laboratory, Remagen (Germany). IR spectra were recorded both as Nujol mulls or in an appropriate solvent on a Perkin-Elmer 684 instrument. ^1H, ^{13}C, and ^{31}P NMR spectra were acquired on a Varian XL-200 spectrometer. $^{31}P\{^1H\}$ NMR shifts were referenced to external 85% H_3PO_4, while $^{13}C\{^1H\}$ and ^1H shifts were referenced to the residual protio signals of deuterated solvents. All data are reported in ppm downfield from $MeSi_4$. All manipulations were performed under oxygen-free nitrogen or argon following conventional Schlenk techniques or by using a Vacuum Atmospheres drybox. Solvents were dried under an appropriate desiccant, deoxygenated, and freshly distilled prior to use. $Mo(\eta^2\text{-}C(O)CH_2SiMe_3)Cl(CO)(PMe_3)_3$[6a] and $ZnCl_2(PMe_3)_2$[6c] were prepared as described previously. Dithiocarbamate and xanthate salts as well as PMe_3 were synthesized according to literature procedures. Sodium dimethyldithiocarbamate was dried by heating at 90 °C at 10^{-2} Torr for 3 days. All other reagents were purchased from commercial suppliers.

$Mo(\eta^2\text{-}C(O)CH_2SiMe_2Ph)Cl(CO)(PMe_3)_3$ (1-Ph). Over a yellow suspension of $MoCl_2(CO)_2(PMe_3)_3$ (0.45 g, 1.0 mmol) and $ZnCl_2(PMe_3)_2$ in diethyl ether, 1.2 mmol of $MgClCH_2SiMe_2Ph$ (1.4 mL, 0.86 M solution) was slowly added. On addition color progresively turns orange-red. The mixture is stirred for 5 h and volatiles removed under vacuum. Extraction in a 1:1 petroleum ether:diethyl ether mixture followed by centrifugation and concentration of the resulting red liquor afforded 0.37 g of **1-Ph** as red crystals (65% yield). Anal. Calcd for $C_{20}H_{40}O_2P_3SiClMo$: C, 42.5; H, 7.1. Found: C, 42.8; H, 7.4. IR (Nujol mull cm^{-1}): 1794 (s), 1507 (m) (υ_{CO}). ^1H NMR (20 °C, C_6D_6): δ 0.52 (s, $SiMe_2$), 1.04 (t, $J_{HP} = 3.0$ Hz, PMe_3), 1.20 (d, $J_{HP} = 8.0$ Hz, 2 PMe_3), 3.20 (s, CH_2), 7.20, 7.58 (m, Ph). $^{31}P\{^1H\}$ NMR (20 °C, C_6D_6): δ 23.3 (d, $J_{PP} = 23$ Hz), 37.5 (t, $J_{PP} = 23$ Hz). $^{13}C\{^1H\}$ NMR (20 °C, CD_3COCD_3): δ −1.7 (s, $SiMe_2$), 15.5 (t, $J_{CP} = 10$ Hz, PMe_3), 20.3 (d, $J_{CP} = 25$ Hz, PMe_3), 39.4 (s, CH_2), 128.5, 129.9, 134.3, 138.7 (s, Ph), 251.4 (dt, $J_{CP} = 31$, 10 Hz, CO), 271.4 (q, $J_{CP} = 12$ Hz, *C*OR).

Preparation of $Mo(C(O)CH_2SiMe_2R)(L-L)CO(PMe_3)_2$ Complexes [L−L = S_2CNMe_2; R = Me (2a-Me, 2d-Me), Ph (2a-Ph); $S_2CN(i\text{-}Pr)_2$ R = Me (3d-Me); $S_2CNC_4H_4$, R = Me (4d-Me); $S_2CO\text{-}i\text{-}Pr$, R = Me (5d-Me), Ph (5d-Ph); $S_2CO\text{-}t\text{-}Bu$, R= Me (6d-Me)]. All these compounds were prepared in a similar way by treating the chloroacyl $Mo(\eta^2\text{-}C(O)CH_2SiMe_2R)Cl(CO)(PMe_3)_3$ with 1.2 equivalents of the sodium or potassium salts of the bidentate ligands in diethyl ether or tetrahydrofuran at room temperature. The synthesis of **2-Ph** is presented as representative example.

A crystalline sample of **1-Ph** (0.56 g, 1.0 mmol) was dissolved in 40 mL of THF and cooled in an ice bath. Anhydrous NaS_2CNMe_2 (0.17 g, 1.2 mmol) was added to the reaction mixture producing a color change from deep red to orange. The resulting suspension was stirred at room temperature for 2h at 0−10 °C and then the volatiles were removed and the resulting residue was extracted with a 1:1 petroleum ether:diethyl ether mixture. Centrifugation followed by concentration of the liquor and cooling at −10 °C afforded **2a-Ph** as orange crystals in 80% yield. From the corresponding chloro-acyl complexes and the appropriate dithiocarbamate or xanthate salts the following compounds were obtained in similar yields. These compounds were isolated as orange-red crystalline solids, except **4d-Me** which is purple, by crystallization of their solutions in petroleum ether−diethyl ether mixtures.

Although some spectroscopic data for the complex $Mo(C(O)CH_2SiMe_3)(S_2CNMe_2)(CO)(PMe_3)_2$ (**2a-Me** and **2d-Me**) have already been reported, for the sake of completeness, their most relevant spectroscopic data are indicated below.

$Mo(C(O)CH_2SiMe_3)(S_2CNMe_2)CO(PMe_3)_2$ (2a-Me). IR (Nujol mull cm^{-1}): 1760 (s), 1615 (m) (υ_{CO}), 1515 (m) (υ_{CN}). ^1H NMR (20 °C, C_6D_6): δ 0.28 (s, $SiMe_3$), 1.42 (d, $J_{HP} = 8.8$ Hz, PMe_3), 2.56 (brs, CH_2), 2.60 (s, NMe_2). $^{31}P\{^1H\}$ NMR (20 °C, C_6D_6): δ 26.7 (brs). $^{13}C\{^1H\}$ NMR (20 °C, C_6D_6): δ 0.5 (s, $SiMe_3$), 15.8 (d, $J_{CP} = 28$ Hz, PMe_3), 38.6 (s, NMe_2). Other carbon resonances were not observed due probably to the low concentration of this compound in solution.

$Mo(\eta^2\text{-}C(O)CH_2SiMe_3)(S_2CNMe_2)(CO)(PMe_3)_2$ (2d-Me). IR (Nujol mull cm^{-1}): 1750 (s), 1490 (m) (υ_{CO}), 1515 (m) (υ_{CN}). ^1H NMR (20 °C, C_6D_6): δ 0.14 (s, $SiMe_3$), 1.56 (t, $J_{HP} = 3.6$ Hz, PMe_3), 3.08 (s, CH_2), 2.77, 2.83 (s, NMe_2). $^{31}P\{^1H\}$ NMR (20 °C, C_6D_6): δ 2.5 (s). $^{13}C\{^1H\}$ NMR (20 °C, C_6D_6): δ −0.7 (s, $SiMe_3$), 15.7 (t, $J_{CP} = 11$ Hz, PMe_3), 37.7 (s, CH_2), 39.2, 39.8 (s, NMe_2), 210.3 (s, S_2C), 238.2 (t, $J_{CP} = 16$ Hz, CO), 275.5 (t, $J_{CP} = 16$ Hz, *C*OR).

$Mo(C(O)CH_2SiMe_2Ph)(S_2CNMe_2)(CO)(PMe_3)_2$ (2a-Ph). Anal. Calcd for $C_{20}H_{37}NO_2P_2S_2SiMo$: C, 41.9; H, 6.4; N 2.4. Found: C, 42.2; H, 6.8; N, 1.6. IR (Nujol mull cm^{-1}): 1785 (s), 1615 (w) (υ_{CO}). ^1H NMR (20 °C, C_6D_6): δ 0.58 (s, $SiMe_2$), 1.37 (d, $J_{HP} = 8.9$ Hz, PMe_3), 2.58 (s, $N(CH_3)_2$), 2.69 (brs, CH_2), 7.25, 7.70 (m, Ph). $^{31}P\{^1H\}$ NMR (20 °C, C_6D_6): δ 27.9 (brs). $^{13}C\{^1H\}$ NMR (20 °C, C_6D_6): δ −0.8 (s, $SiMe_2$), 15.5 (d, $J_{CP} = 28$ Hz, PMe_3), 38.8 (s, $N(CH_3)_2$), 128.3, 129.0, 134.5, 140.2 (s, Ph). Other carbon resonances were not observed, probably due to the low concentration of this compound in solution.

$Mo(\eta^2\text{-}C(O)CH_2SiMe_2Ph)(S_2CNMe_2)(CO)(PMe_3)_2$ (2d-Ph). IR (THF cm^{-1}): 1775 (s) (υ_{CO}). ^1H NMR (20 °C, C_6D_6): δ 0.46 (s, $SiMe_3$), 1.52 (t, $J_{HP} = 3.6$ Hz, PMe_3), 2.77, 2.82 (s, $N(CH_3)_2$), 3.28 (s, CH_2), 7.19, 7.50 (m, Ph). $^{31}P\{^1H\}$ NMR (20 °C, C_6D_6): δ 3.6 (s). $^{13}C\{^1H\}$ NMR (20 °C, C_6D_6): δ −1.8 (s, $SiMe_2$), 15.9 (t, $J_{CP} = 11$ Hz, PMe_3), 37.1 (s, CH_2), 39.5, 40.1 (s, $N(CH_3)_2$), 128.2, 129.6, 134.1, 138.1 (s, Ph), 210.5 (s, S_2C), 238.7 (t, $J_{CP} = 14$ Hz, CO), 275.9 (t, $J_{CP} = 16$ Hz, *C*OR).

$Mo(\eta^2\text{-}C(O)CH_2SiMe_3)(S_2CN\text{-}i\text{-}Pr_2)(CO)(PMe_3)_2$ (3d-Me). Anal. Calcd for $C_{19}H_{43}NO_2P_2S_2SiMo$: C, 40.2; H, 7.6, N, 2.5.

Found: C, 40.5; H, 7.6, N, 2.7. IR (Nujol mull cm^{-1}): 1760 (s), 1475 (m) (υ_{CO}), 1490 (m) (υ_{CN}). ^1H NMR (20 °C, C_6D_6): δ 0.12 (s, $SiMe_3$), 1.19 (brs, $CH(CH_3)_2$), 1.56 (t, $J_{HP} = 3.5$ Hz, PMe_3), 3.05 (s, CH_2), 4.60 (brs, CH). $^{31}P\{^1H\}$ NMR (20 °C, C_6D_6): δ 4.8 (s). $^{13}C\{^1H\}$ NMR (20 °C, C_6D_6): δ −0.6 (s, $SiMe_3$), 15.7 (t, $J_{CP} = 11$ Hz, PMe_3), 19.3, 19.7 (s, $CH(CH_3)_2$), 38.0 (s, CH_2), 50.0, 50.8 (s, CH), 209.7 (t, $J_{CP} = 7$ Hz, S_2C), 237.9 (t, $J_{CP} = 14$ Hz, CO), 276.0 (t, $J_{CP} = 16$ Hz, *C*OR).

Mo(η^2-C(O)CH_2SiMe_3)($S_2CNC_4H_4$)(CO)(PMe_3)$_2$ (4d-Me). Anal. Calcd for $C_{17}H_{33}NO_2P_2S_2SiMo$: C, 38.3; H, 6.2, N, 2.6. Found: C, 37.8; H, 5.9, N, 2.6. IR (Nujol mull cm^{-1}): 1780 (s), 1465 (m) (υ_{CO}), 1485 (m) (υ_{CN}). ^1H NMR (20 °C, C_6D_6): δ 0.08 (s, $SiMe_3$), 1.39 (t, $J_{HP} = 3.7$ Hz, PMe_3), 3.00 (s, CH_2), 6.10, 7.80 (t, CH). $^{31}P\{^1H\}$ NMR (20 °C, C_6D_6): δ 5.8 (s). $^{13}C\{^1H\}$ NMR (20 °C, C_6D_6): δ −0.6 (s, $SiMe_3$), 15.8 (t, $J_{CP} = 12$ Hz, PMe_3), 37.8 (s, CH_2), 112.9, 117.9 (s, CH), 208.7 (t, $J_{CP} = 8$ Hz, S_2C), 237.1 (t, $J_{CP} = 15$ Hz, CO), 276.0 (t, $J_{CP} = 16$ Hz, *C*OR).

Mo(η^2-C(O)CH_2SiMe_3)(S_2CO-*i*-Pr)(CO)(PMe_3)$_2$ (5d-Me). Anal. Calcd for $C_{16}H_{36}NO_2P_2S_2SiMo$: C, 35.5; H, 6.8. Found: C, 35.3; H, 6.8. IR (Nujol mull cm^{-1}): 1795 (s), 1485 (m) (υ_{CO}). ^1H NMR (20 °C, C_6D_6): δ 0.21 (s, $SiMe_3$), 1.07 (d, $J_{HH} = 6.2$ Hz, $CH(CH_3)_2$), 1.44 (t, $J_{HP} = 3.6$ Hz, PMe_3), 3.02 (s, CH_2), 5.34 (h, $J_{HH} = 6.2$ Hz, CH). $^{31}P\{^1H\}$ NMR (20 °C, C_6D_6): δ 5.2 (s). $^{13}C\{^1H\}$ NMR (20 °C, C_6D_6): δ 1.0 (s, $SiMe_3$), 15.7 (t, $J_{CP} = 11$ Hz, PMe_3), 21.4 (s, $CH(CH_3)_2$), 37.8 (s, CH_2), 74.5 (s, CH), 222.3 (t, $J_{CP} = 6$ Hz, S_2C), 236.7 (t, $J_{CP} = 15$ Hz, CO), 276.7 (t, $J_{CP} = 16$ Hz, *C*OR).

Mo(η^2-C(O)CH_2SiMe_2Ph)(S_2CO-*i*-Pr)(CO)(PMe_3)$_2$(5d-Ph). Satisfactory elemental analysis was precluded by its thermal instability. IR (Nujol mull cm^{-1}): 1800 (s), 1465 (m) (υ_{CO}). ^1H NMR (20 °C, C_6D_6): δ 0.40 (s, $SiMe_3$), 1.10 (d, $J_{HH} = 6.2$ Hz, $CH(CH_3)_2$), 1.44 (t, $J_{HP} = 3.7$ Hz, PMe_3), 3.23 (s, CH_2), 5.40 (h, $J_{HH} = 6.2$ Hz, CH), 7.20, 7.46 (m, Ph). $^{31}P\{^1H\}$ NMR (20 °C, THF/CD_3COCD_3): δ 9.7 (s). $^{13}C\{^1H\}$ NMR (20 °C, C_6D_6): δ −2.3 (s, $SiMe_2$), 15.5 (t, $J_{CP} = 11$ Hz, PMe_3), 21.3 (s, $CH(CH_3)_2$), 36.9 (s, CH_2), 74.5 (s, CH), 127.9, 129.4, 133.7, 137.4 (s, Ph), 222.3 (t, $J_{CP} = 7.8$ Hz, S_2C), 237.1 (t, $J_{CP} = 13$ Hz, CO), 276.6 (t, $J_{CP} = 15$ Hz, *C*OR).

Mo(η^2-C(O)CH_2SiMe_3)(S_2CO-*t*-Bu)(CO)(PMe_3)$_2$ (6d-Me). Anal. Calcd for $C_{17}H_{38}NO_2P_2S_2SiMo$: C, 37.8; H, 7.0. Found: C, 38.0; H, 7.1. IR (Nujol mull cm^{-1}): 1760 (s), 1485 (m) (υ_{CO}). ^1H NMR (20 °C, C_6D_6): δ 0.12 (s, $SiMe_3$), 1.56 (t, $J_{HP} = 3.7$ Hz, PMe_3), 1.63 (s, CMe_3), 3.20 (s, CH_2). $^{31}P\{^1H\}$ NMR (20 °C, C_6D_6): δ 5.4 (s). $^{13}C\{^1H\}$ NMR (20 °C, C_6D_6): δ −0.7 (s, $SiMe_3$), 15.7 (t, $J_{CP} = 11$ Hz, PMe_3), 21.4 (s, $C(CH_3)_3$), 37.8 (s, CH_2), 86.9 (s, $C(CH_3)_3$), 222.1 (t, $J_{CP} = 6$ Hz, S_2C), 236.9 (t, $J_{CP} = 14$ Hz, CO), 276.5 (t, $J_{CP} = 15$ Hz, *C*OR).

Computational Details. All calculations were performed with the GAUSSIAN 94 series of programs.[31] A molecular orbital ab initio method with introduction of correlation energy through the Moller−Plesset (MP) perturbation approach,[32] excluding excitations concerning the lowest energy electrons (frozen core approach), was applied. Effective core potentials (ECP) were used to represent the 28 innermost electrons of the metal atom[33a] as well as the 10 electron core of the phosphorus, sulfur, and silicon atoms.[33b] Geometry optimizations were carried out at the second level of the Møller−Plesset theory (MP2) with a basis set of valence double-ζ quality for all the atoms. It has already been shown that the computed MP2 geometries in agostic complexes are in excellent agreement with experimental neutron diffraction data.[34] Two different basis sets were used. Basis set I was used in most calculations, including all geometry optimizations. In basis set I, the basis for molybdenum, phosphorus, sulfur, and silicon was that associated with the pseudopotential[32] with standard LANL2DZ contraction schemes.[31] For the other atoms the 6-31G basis set was used.[35]

Basis set II, much more extended than basis set I, was used to check the basis set dependence of the computed energies through single-point calculations on structures frozen at the geometry obtained with basis set I. Basis set II was obtained from basis set I by adding a shell of polarization functions to all atoms, i.e., a p shell on hydrogen atoms[35a,b] a d shell on carbon, nitrogen, oxygen, phosphorus, and sulfur atoms,[35a−d] and an f shell on the molybdenum atom.[35e]

All the geometric parameters were optimized to find the most stable structure for each compound. To evaluate the energy differences between agostic and anagostic geometries, optimizations were performed for the least stable structures keeping fixed the value of the Mo−C_α-C_β at 109.4° in **12** and 120° in **8**. Symmetry restrictions (Cs) were introduced in the optimizations when possible.

X-ray Structure Determination of 2a-Me. A summary of the fundamental crystal data is given in Table 1. A crystal of **2a-Me** was coated with an epoxy resin and mounted in a Kappa diffractometer. The cell dimensions were refined by least-squares fitting of the values of 25 reflections. The intensities were corrected for Lorentz and polarization effects. Scattering factors for neutral atoms and anomalous dispersion corrections for Mo, P, and S were taken from ref 36. The structures were solved by Patterson and Fourier methods. An empirical absorption correction[37] was applied at the end of the isotropic refinement. Final mixed refinement with unit weights and fixed isotropic factors and coordinates for H atoms, except for H(31) and H(32) for which the corresponding coordinates were refined, led to final values of $R = 0.037$ and $R_w = 0.055$. The final values of the positional parameters are given in Table 2. Most of the calculations were carried out with the X-ray 80 system.[38]

Acknowledgment. We acknowledge financial support from the DGES (Project No PB95-0639-CO2-01) and the DGICYT (grant No. PB94-1436). We also acknowledge Junta de Andalucía for the award of research fellowships. The use of computational facilities of the Centre de Supercomputació i Comunicacions de Catalunya (C^4) is gratefully appreciated. Prof. O. Eisenstein (Montpellier) is acknowledged for fruitful discussions.

Supporting Information Available: Tables of atomic and thermal parameters for **2a-Me**. This material is available free of charge via the Internet at http://pubs.acs.org.

OM9807248

(31) Frisch, M. J.; Trucks, G. W.; Schlegel, H. B.; Gill, P. M. W.; Johnson, B. G.; Robb, M. A.; Cheeseman, J. R.; Keith, T. A.; Petersson, G. A.; Montgomery, J. A.; Raghavachari, K.; Al-Laham, M. A.; Zakrzewski, V. G.; Ortiz, J. V.; Foresman, J. B.; Cioslowski, J.; Stefanov, B. B.; Nanayakkara, A.; Challacombe, M.; Peng, C. Y.; Ayala, P. Y.; Chen, W.; Wong, M. W.; Andrs, J. L.; Replogle, E. S.; Gomperts, R.; Martin, R. L.; Fox, D. J.; Binkley, J. S.; De Frees, D. J.; Baker, J.; Stewart, J. P.; Head-Gordon, M.; Gonzalez, C.; Pople, J. A. *Gaussian 94*; Gaussian Inc.: Pittsburgh, PA, 1995.

(32) Moller, C.; Plesset, M. S. *Phys. Rev.* **1934**, *46*, 618.

(33) (a) Hay, P. J.; Wadt, W. R. *J. Chem. Phys.* **1985**, *82*, 299. (b) Wadt, W. R.; Hay, P. J. J. *Chem. Phys.* **1985**, *82*, 284.

(34) Weiss, H.; Haase, F.; Ahlrichs, R. *Chem. Phys. Lett.* **1992**, *194*, 492.

(35) (a) Hehre, W. J.; Ditchfield, R.; Pople, J. A. *J. Chem. Phys.* **1972**, *56*, 2257. (b) Hariharan, P. C.; Pople, J. A. *Theor. Chim. Acta* **1973**, *28*, 213. (c) Francl, M. M.; Pietro, W. J.; Hehre, W. J.; Binkley, J. S.; Gordon, M. S.; Defrees, D. J.; Pople, J. A. *J. Chem. Phys.* **1982**, *77*, 3654. (d) Hullwarth, A.; Buhhme, M.; Dapprich, S.; Ehlers, A. W.; Gobbi, A.; Jonas, V.; Kuhler, K. F.; Stegmann, R.; Veldkamp, A.; Frenking, G. *Chem. Phys. Lett.* **1993**, *208*, 237. (e) Ehlers, A. W.; Buhme, M.; Dapprich, S.; Gobbi, A.; Hullwarth, A.; Jonas, V.; Kuhler, K. F.; Stegmann, R.; Veldkamp, A.; Frenking, G. *Chem. Phys. Lett.* **1993**, *208*, 111.

(36) *International Tables for X-Ray Crystallography*; Kynoch Press: Birmingham, UK, 1974; Vol. IV, pp 72−98.

(37) Walker, N.; Stuart, D. *Acta Crystallogr.* **1983**, *A39*, 158.

(38) Stewart, J. M. The X-ray 80 System; Computer Science Center, University of Maryland: College Park, MD, 1985.